Wave vector dependence of x-ray beam induced dynamics in sodium silicate glasses

E. Alfinelli,[1,*] F. Caporaletti,[2,3] A. Martinelli,[4] G. Monaco,[5] M. Sprung,[6] and G. Baldi[1,†]

[1]*Department of Physics, University of Trento, 38123 Povo, Trento, Italy*

[2]*Van der Waals-Zeeman Institute, Institute of Physics, University of Amsterdam, 1098XH Amsterdam, The Netherlands*

[3]*Faculty of Science, Université libre de Bruxelles, Bd de la Plaine 2, 1050 Ixelles, Belgium*

[4]*Laboratoire Charles Coulomb, Université de Montpellier, CNRS, Pl. Eugéne Bataillon, 34095 Montpellier, France*

[5]*Department of Physics and Astronomy 'Galileo Galilei', University of Padova, 35131 Padova, Italy*

[6]*Hasylab at DESY, Notkestraße 85, D-22607 Hamburg, Germany*

(Received 21 May 2024; revised 8 August 2024; accepted 10 September 2024; published 25 September 2024)

We have probed the atomic dynamics of two sodium silicate glasses in a wide wave vector range by means of x-ray photon correlation spectroscopy. The wide angle setup has been modified to cover a Q range that extends to small angles, close to the range normally covered by the usual small-angle x-ray scattering configuration. During irradiation, the oxide samples undergo a transformation to a new amorphous state with different structural and dynamical properties. The observed dynamics before and after the structural transformation shows the presence of de Gennes narrowing. In the low wave vector region, the dynamics is affected by a ballisticlike motion at low absorbed doses, while the glass obtained after prolonged irradiation has a Q-independent relaxation time. This observation strengthens the interpretation of the new amorphous phase as a rejuvenated glass that lies in a higher-energy region of the potential landscape.

DOI: 10.1103/PhysRevB.110.094207

I. INTRODUCTION

Glasses are disordered systems without long-range order, and their low-frequency response can be described by treating the solid as a continuous elastic network. It would be thus natural to assume the Debye approximation holds true as long as the observations correspond to length scales larger than the microscopic structure, as in crystalline solids. It is, instead, well known that the Debye model does not capture the low-temperature thermal properties of glasses [1,2], and the usual elasticity theory cannot describe the vibrational spectrum when the length scale falls below some tens of interatomic distances [3–6]. The typical vibrational features appearing at terahertz frequencies can be interpreted as arising from heterogeneities in the elastic properties of the material with a typical size of a few nanometers [7–10]. Some evidence from numerical simulations and experiments suggests that these fluctuating elasticity regions arise from the dynamical heterogeneities characterizing the structural relaxation process of the supercooled liquid close to the glass transition [11,12].

Authors of several works have focused on the investigation of the physical properties in the medium-range order, as for example inelastic x-ray [3–6,10] or neutron scattering [13–15] and numerical simulation studies. The difficulty in analyzing these length scales stems from the lack of experimental probes: X-ray photon correlation spectroscopy (XPCS) is a viable technique to capture the dynamics at those scales. The method is designed to probe the long time dynamics of the structural relaxation in viscous liquids and glasses from the determination of the density fluctuations at interatomic distances. In the case of low-temperature viscous liquids, glasses at the glass transition temperature, and biological systems, the time correlation function usually follows a stretched exponential decay $e^{-(t/\tau)^{\beta}}$, known as the Kohlrausch-Williams-Watts (KWW) model [16,17]. The stretching parameter β, with $0 < \beta < 1$, is compatible with slow cooperative dynamics characterized by a heterogeneous distribution of relaxation times in the different rearranging regions [12,18]. However, light and x-ray scattering experiments on the aging of soft materials have detected microscopic dynamics which can be faster than exponential [19–22]. The shape of the correlation function with $\beta > 1$, usually termed compressed exponential, has been interpreted as the signature of a dynamic that proceeds through the release of the stress accumulated inside the material via the rupture of network connections [23,24]. In this regime, the wave vector dependence of the relaxation time indicates a ballistic ($\tau \propto 1/Q$) rather than a diffusive dynamic ($\tau \propto 1/Q^2$) [25,26].

Similar observations are obtained with XPCS experiments on oxide glasses. The intense x-ray fluxes available at synchrotron sources activate atomic motion in the probed sample, inducing a fast decorrelation even at temperatures well below the glass transition, in the deep glassy state [25–33]. The accepted interpretation of the mechanism giving rise to this beam induced motion is based on the radiolysis process. The x-ray photon interacts with matter and generates a cascade of electrons. The ones with lower energy localize on self-trapped excitons that distort the glass network, creating point defects. Some bonds are removed in the process, stimulating the

*Contact author: erica.alfinelli@unitn.it

†Contact author: giacomo.baldi@unitn.it

 ©2024 American Physical Society

motion of the nearby atoms of the disordered network [26]. The observed decorrelation time is inversely proportional to the beam flux and can consequently be interpreted as the x-ray dose necessary to rearrange the entire scattering volume. At low absorbed doses, i.e., delivered energy per unit mass, the phenomenon is reversible because the sample structure does not vary in an appreciable way, as revealed by the static structure factor [25,32]. In those conditions, the system is in a definite initial state that we call *pristine*. In this regime, the beam induced dynamics of pure vitreous silica shows a peculiar wave vector dependence, with $\tau \propto Q^{-0.5}$ [25,26]. Such hyperdiffusive behavior together with the compressed shape of the relaxation function implies that the atomic displacements are described by a long-tailed Levy-stable distribution in which the long displacements are favored, stimulated by the accumulation of radiolytic events [26]. The reversibility is lost in the case of long irradiation times where the radiolysis causes a change in the structure of the glass and induces the transformation to a different amorphous state [33]. We will refer to this new state as the *new amorphous* in what follows (the new state is also called *fully irradiated glass* in a recent paper by Martinelli *et al.* [34]).

The evolution of the glass under high radiation doses has been investigated in two recent papers [33,34]. In one [33], we have studied the dose evolution of the structure and dynamics of a selection of sodium silicates glasses and of pure boron oxide at a fixed exchanged wave vector, $Q = 1.6\,\text{Å}^{-1}$. This paper complements the study with the investigation of the wave vector dependence of the dynamics for two compositions of the sodium silicates. We have analyzed these glasses in the pristine and new amorphous states, and we have exploited a dedicated setup to probe the low wave vector region between 0.2 and 0.5 Å^{-1}, a regime intermediate between the standard small- and wide-angle configurations.

II. METHODS

The samples are sodium silicates $(Na_2O)_x(SiO_2)_{(1-x)}$ with $x = 20\%$ (Na20) and $x = 43\%$ (Na43) of sodium oxide, two of the samples studied in Ref. [33]. The samples have been prepared by melting the silica and the sodium carbonate powders into an alumina crucible (Coors™) at temperatures above the melting point and by quenching them in air at room temperature. The transparent materials have been prepared in the shape of disks of ∼5 mm and optically polished to a thickness of ∼50 μm to achieve good contrast in the correlation functions. Table I reports some physical properties of the two samples.

TABLE I. Physical properties of the samples. Na20 (Na40) refers to the glass with 20% (40%) of Na_2O. The attenuation length is calculated at 8.25 keV, the x-ray energy of the XPCS experiment. The uncertainty on the thickness comes from the roughness of the surface profile measured in transmission geometry.

Sample tag	Thickness (μm)	Density (g/cm^3)[35]	Attenuation length (μm)[36]	T_g (K) [37]
Na20	49(5)	2.38	140.8	750
Na43	46(1)	2.545	143.1	670

The XPCS experiment (No. I-20180946) was carried out at the P10 beamline of the Petra III synchrotron in Hamburg, Germany. Two different beamline configurations have been exploited to cover a large Q range. We have used the standard wide-angle configuration for the Q range between 0.5 and 2.5 Å^{-1}, while for the low-Q region (0.2 to 0.5 Å^{-1}), we have exploited a new setup where the space between the sample and the detector is kept under vacuum. The partially coherent x-ray beam of energy 8.25 keV is focused at the sample stage to a spot of $3 \times 2\,\mu\text{m}^2$ of full width at half maximum (FWHM) and with a photon flux of 4.2×10^{10} ph/s. In the wide-angle configuration, the sample is mounted into a vacuum chamber with a Kapton window on the detector side. This window is removed for the low-Q investigation. The scattered radiation is recorded by a two-dimensional (2D) detector (Eiger4M from Dectris) which counts 2070 × 2167 pixels, and it is fixed at the end of a vacuum tube and mounted on a goniometer. The detector is placed 1.8 m away from the sample stage to match the speckles with the pixels dimension of $75 \times 75\,\mu\text{m}^2$. We collected measurements at room temperature and at different scattering angles θ to get a wide range of scattering wave vectors defined as $Q = (4\pi/\lambda)\sin(\theta/2)$, where λ is the x-ray beam wavelength. The relation is not linear, and so the detector covers a wider Q range when placed at low angles. Thus, we have divided the area into a different number of regions depending on the scattering angle to achieve a Q resolution of $\delta Q/Q \leqslant 20\%$. The measurement at every angle was repeated a minimum of three times except when the detector was placed at the highest angles because the statistics of the single measurement was sufficient to have a reliable result. Every repetition has been performed on a fresh spot on the sample. The dose rate has been calculated for every sample as $d_r = \epsilon \cdot A/N$. Here, ϵ is the photon energy of the probe, N the number of atoms in the scattering volume, and A the absorbed flux calculated from the transmitted one $\phi \cdot T$, $A = \phi \cdot (1 - T)$, with ϕ the photon flux. The dose rates for the two samples are d_r(Na20) = 6.5 eV atom^{-1} s^{-1} and d_r(Na43) = 6.0 eV atom^{-1} s^{-1}. The total dose for every measurement can be computed as $D = d_r \cdot t_w$, where t_w is the total exposure time of the sample.

The data have been processed by following the multi-speckle approach [38]. The method is based on the calculation of the two times correlation function (TTCF), $G(Q, t_1, t_2)$, defined as the instantaneous correlation of the intensity of a region of interest of the detector corresponding to a given value of the scattering wave vector:

$$G(Q, t_1, t_2) = \frac{\langle I(t_1)I(t_2)\rangle_p}{\langle I(t_1)\rangle_p \langle I(t_2)\rangle_p}, \tag{1}$$

where $\langle\ \rangle_p$ is the average over pixels subtending the same scattering wave vector Q. Here, $I(t)$ is the intensity recorded on a single pixel at time t. The TTCF of the Na43 sample at $Q = 1.6\,\text{Å}^{-1}$ is shown in the upper panel of Fig. 1. The autocorrelation function is calculated by averaging in time the TTCF, taking advantage of both spatial and temporal evolution of the speckles. The autocorrelation function is connected to the intermediate scattering function (ISF) $F(Q, t)$, thanks to the Siegert relation:

$$g^{(2)}(Q, t) = y_0 + \mathcal{C}_Q |F(Q, t)|^2, \tag{2}$$

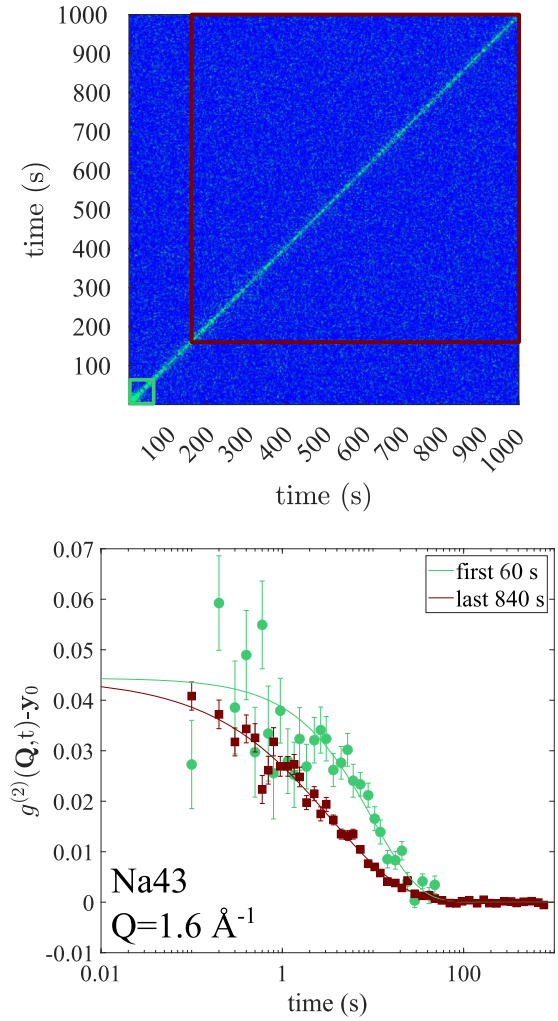


FIG. 1. (upper) Two times correlation function (TTCF) of the sample $(Na_2O)_{0.43}(SiO_2)_{0.57}$ measured at $Q = 1.6\,\text{Å}^{-1}$. The green and brown squares show the temporal windows in which the autocorrelation functions of the right side have been computed. (lower) Autocorrelation functions calculated from the TTCF on the left at different irradiation times. Green dots refer to the dynamics over the first 60 s of the irradiation. Brown squares show the autocorrelation points on the last 840 s.

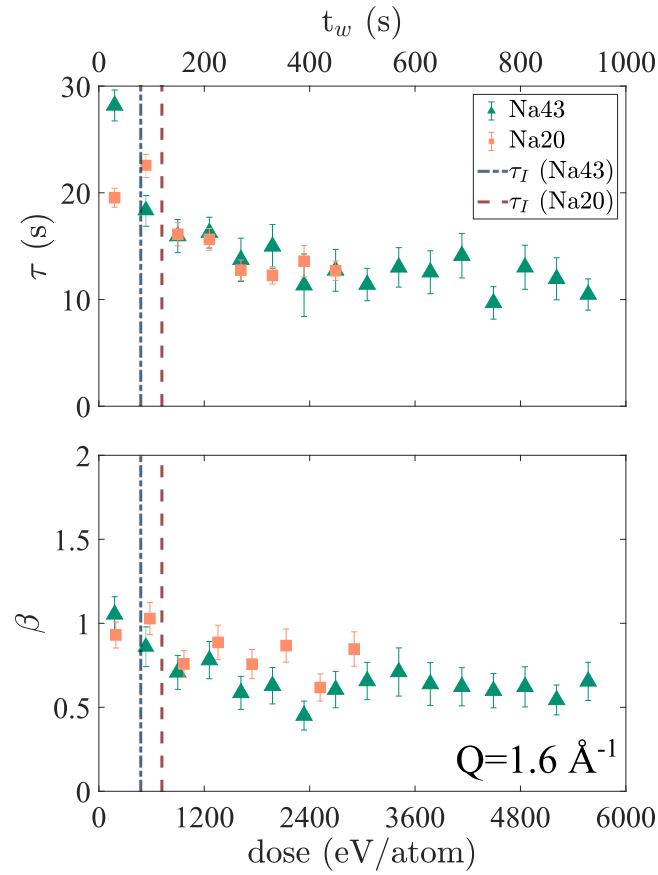


FIG. 2. (upper) Observed relaxation time as a function of the absorbed dose for Na43 (green triangles) and Na20 (orange squares) samples at scattering wave vector $Q = 1.6\,\text{Å}^{-1}$. (lower) The corresponding β parameter. The characteristic time τ_I is reported as a line for both the investigated samples (blue for Na43 and brown for Na20). The axis on the top reports the exposure time (t_w) which is related to the absorbed dose by means of the dose rate d_r.

where y_0 is a baseline, and $\mathcal{C}_Q$ is the experimental contrast. The typical values of the baseline are compatible with zero within uncertainty, while $\mathcal{C}_Q$ has a marked Q dependence due to the limited longitudinal coherence of the x-ray beam, with values of only a few percent at wide angles (see the lower panel of Fig. 1).

The ISF is modeled via the KWW equation:

$$F(Q,t) = f_Q e^{-(t/\tau_Q)^{\beta_Q}}. \tag{3}$$

Here, τ_Q is the characteristic relaxation time, β_Q gives the shape of the exponential, and f_Q represents the nonergodicity parameter. This parameter describes the decrease in correlation taking place at times shorter than those accessible in the measurement [39–41]. The TTCF shows the evolution of the dynamics as a function of time. The x-ray dose accumulation at this wave vector gives rise to an acceleration of the induced dynamics as visible in the narrowing of the matrix diagonal. More in detail, we followed quantitatively this evolution by calculating the ISF in small submatrices with sides of 60 s that we located along the diagonal of the TTCF. Two examples of submatrices are marked by colored squares in the upper panel of Fig. 1. The resulting relaxation time and β value from the KWW model as a function of the absorbed dose are shown in Fig. 2.

The evolution of the dynamics is accompanied by an exponential variation of the scattered intensity [33] that can be described in the following way:

$$I(t_w) = I_\infty + (I_0 - I_\infty)e^{-(t_w/\tau_I)}, \tag{4}$$

where I_0 and I_∞ are, respectively, the initial and final values of intensity, and τ_I is the typical time of the intensity variation. The calculated values of τ_I at $Q = 1.6\,\text{Å}^{-1}$ are reported, in units of absorbed dose, as vertical lines in Fig. 2 for both samples. The observed relaxation and decay times of the intensity have similar values, making it challenging to investigate the dynamics before the system undergoes the structural modification. This structural variation induces modifications in the observed dynamics with an accelerated

relaxation time and a correlation curve that becomes stretched. We decided to compute the temporal average of the TTCF where the intensity is sufficiently stable in time, specifically in the pristine glass (low doses) and in the irradiated one (high doses). The two regions are highlighted with green and brown squares in the upper panel of Fig. 1. Examples of the correlation curves for the two dose regimes are instead reported in the bottom panel of the same figure: green dots for the short irradiation part and brown squares for the long one. The points of the correlation curve for short exposure times, in the pristine glass, are subject to higher uncertainties, and the curve is truncated at only twice the characteristic decay time τ_Q. A good signal-to-noise ratio requires either the use of a large detector region, at the expenses of the Q resolution, or a total integration time sufficiently longer than τ_Q. At short exposures, the decay time of the intensity is a few times the observed XPCS relaxation. This necessarily implies a truncated correlation curve with lower statistical accuracy in the low wave vector region. As a compromise, we have decided to analyze the dynamics for an irradiation time window below $0.75\tau_I$ so that what we call a pristine glass is indeed already undergoing some structural variation. This choice may affect the shape of the correlation curves because an average over a nonstationary dynamic can decrease the value of β as compared with the value expected in the real pristine glass. The high-dose regime is considered from $2\tau_I$ onward.

III. RESULTS

The scattered intensity profiles in Figs. 3(a) and 3(c) show how the physical and structural properties of the silicate glasses are related to the concentration of alkali modifiers [37]. Addition of alkali metals, such as sodium ions, in the v-SiO_2 network induces the breakage of covalent bonds and the creation of nonbridging oxygen species (NBO), which are oxygen atoms with a dangling bond for the presence of a nearby cation. In this depolymerized network, the sodium cations form channels [42] and change the connectivity and the structure of the initial network. As an example, in Fig. 3(a), the Na20 sample has a pronounced peak ∼1.6 $Å^{-1}$, the position of the first sharp diffraction peak (FSDP) of v-SiO_2, and a faint shoulder for $Q \sim 2.3$ $Å^{-1}$. An increase of sodium concentration leads to a reverse of the intensity ratio between these two peaks in the case of the Na43 sample, leading to a higher intensity at $Q \sim 2.3$ $Å^{-1}$ [see Fig. 3(c)]. The wave vector dependence of the scattered intensity is reported in Figs. 3(a) and 3(c) at the two levels of irradiation, short exposure (pristine glass, empty points) and long exposure (new amorphous state, full points). An intensity variation is present in both samples with a reduction of the FSDP and an increase at low wave vectors giving rise to a broadening of the static structure factor. The relative intensity variation on the peak is ∼5% for the Na20 sample and 2% in the case of Na43, leading to a higher uncertainty in the determination of the parameter τ_I for the latter. The complete relative variation of the intensity on the entire explored wave vector range is reported in Figs. 3(b) and 3(d) for both samples. The dose dependence on the FSDP can be found in Ref. [33]. The structural evolution suggests that the final amorphous state has an increased

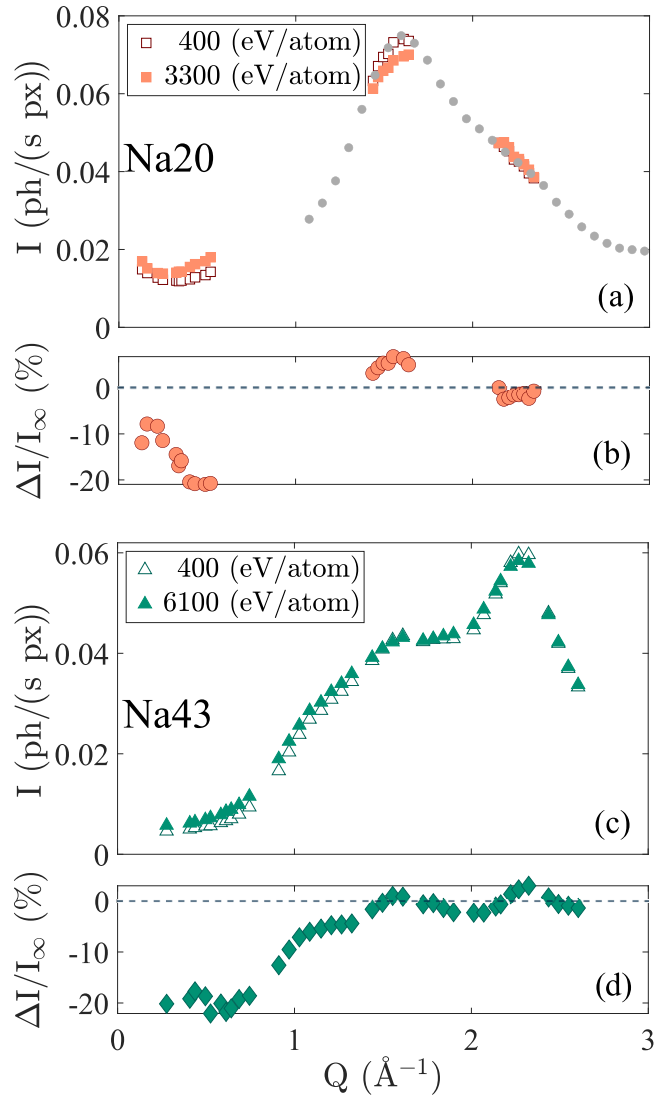


FIG. 3. Scattered intensity as a function of the wave vector Q at two irradiation doses for (a) Na20 and (c) Na43. The gray points in (a) are scattered intensity data recorded with only 1 s of exposure. They are added to show the complete intensity profile of Na20. Relative variation of the intensity as a function of the wave vector for samples (b) Na20 and (d) Na43. The variation is calculated as $\Delta I/I_\infty = (I_0 - I_\infty)/I_\infty$, where I_0 is the intensity of the pristine state and I_∞ the intensity of the final amorphous state. The dotted line highlights the position of zero variation in the intensity.

disorder. We also note that an increase of the small-angle signal is an indication of an increase in the fictive temperature of the glass [43], in agreement with the idea that the glass exposed to a high level of radiation is rejuvenated with respect to the pristine glass. The scattered intensity is lower for the sample with higher sodium concentration at almost all probed wave vectors, affecting the statistical accuracy of the XPCS measurement, making the measurement at low wave vectors, below 0.6 $Å^{-1}$, quite challenging. We have increased the robustness of the fit of the XPCS correlation function of Na43 in this low-Q range by fixing the contrast parameter at the value obtained from the analysis of the Na20 sample at the same wave vectors. It is worth noticing that this choice does

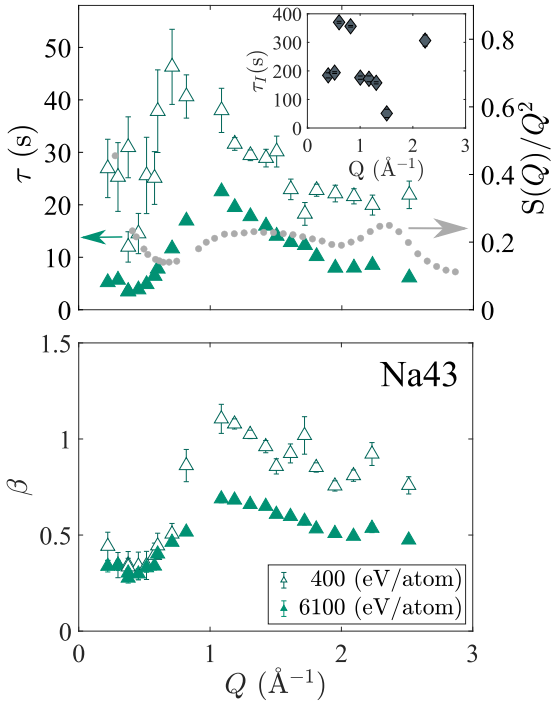


FIG. 4. Dynamics as a function of the wave vector for the Na43 sample. (upper) Relaxation time as a function of the wave vector at two absorbed doses: low doses (empty green triangles) and high doses (full green triangles). The ordinate axis on the right reports the scale of $S(Q)/Q^2$ (gray full dots). Inset: The characteristic time for the variation of the static structure factor as a function of the wave vector. (lower) β parameter as a function of the wave vector calculated at the same doses of the upper panel.

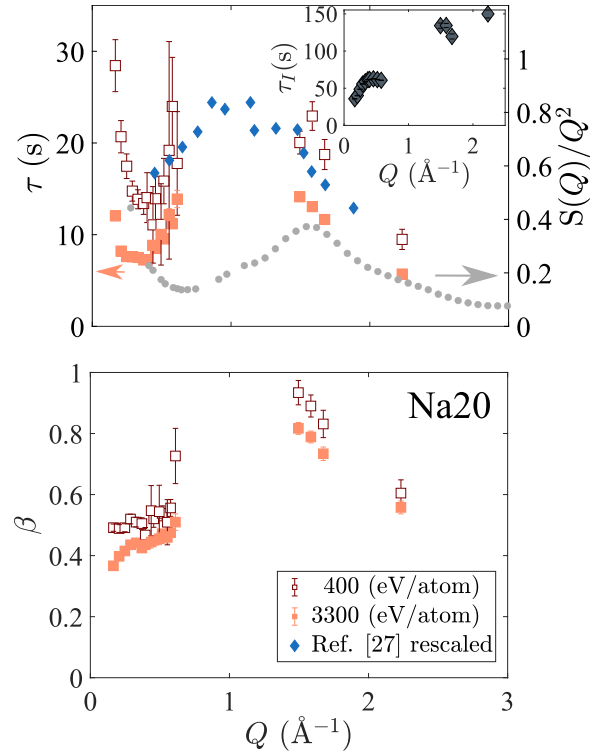


FIG. 5. Dynamics as a function of the wave vector for the Na20 sample. (upper) Relaxation time as a function of the wave vector for two absorbed doses: low doses (empty brown squares) and high doses (full orange squares). The blue diamonds are relaxation time data from Ref. [27]. They have been rescaled by a factor 10 to fit with the data in this paper. The ordinate axis on the right reports the scale of $S(Q)/Q^2$ (gray full dots). Inset: The characteristic time for the variation of the static structure factor as a function of the wave vector. (lower) β parameter as a function of the wave vector calculated at the same doses of the upper panel.

not account for the different nonergodicity factor f_Q between the two samples. Indeed, a source of decorrelation is related to the vibrational dynamics of the glass, and a change in the sodium oxide concentration leads to a different amount of vibrations. Inelastic x-ray scattering (IXS) experiments have revealed that the nonergodicity parameter varies as a function of the temperature and the exchanged wave vector [10,40,41]. At Q's corresponding to the FSDP, f_Q is very close to 1, while at low Q's, the f_Q parameter depends on the glass fragility as $f_Q^{-1} = 1 + \alpha T/T_g$ [40]. We estimate the variation in the contrast between the two samples due to the small difference in f_Q to be lower than 5%, which is within the uncertainty of the fit.

The values of the decorrelation time and the β parameter are shown in Fig. 4 for the Na43 sample as a function of the wave vector for the two irradiation levels, short (empty triangles) and long exposure (full triangles), together with the quantity $S(Q)/Q^2$ derived from the scattered intensity of the pristine glass (absolute scale on the right axis). The scales of τ_Q and $S(Q)/Q^2$ are compared with each other using an arbitrary scaling factor. The relaxation time shows a mild wave vector dependence and decreases at high absorbed doses. The decorrelation time must be viewed as the time required to accumulate the x-ray dose necessary to force the change in the atomic configuration of the entire scattering volume, as anticipated in the introduction. The x-ray dose accumulated in τ_Q is in general different from system to system, and it is related to the topology of the glass network [33].

The inset of the upper panel shows the characteristic time for the variation of the static structure factor, which is a few times longer than the decorrelation time. The quantity is affected by significant noise because the intensity variation is quite small, as shown in Figs. 3(b) and 3(d). The β parameter is affected by a marked variation as the dose is increased, as shown in the lower panel of Fig. 4. The correlation curve has β slightly above 1 in the pristine glass for $Q \sim 1\,\text{Å}^{-1}$, and becomes stretched at high absorbed doses. In the low-Q range, on the contrary, the curve appears stretched from the beginning. The dynamics of the Na20 sample is shown in Fig. 5. Here, we have measured less points at wide angles with respect to the other sample, while we managed to obtain data with higher quality in the low wave vector region. In the upper panel of the figure, we plot the quantity $S(Q)/Q^2$ together with the relaxation time obtained in a previous measurement where the absolute dose to the sample was not monitored [27]. These data have been rescaled by an arbitrary factor to compare the Q evolution with that in this paper. The high-Q region shows a mild Q dependence, analogous to that of the Na43 sample, while the low-Q behavior is marked by a fast decrease of the

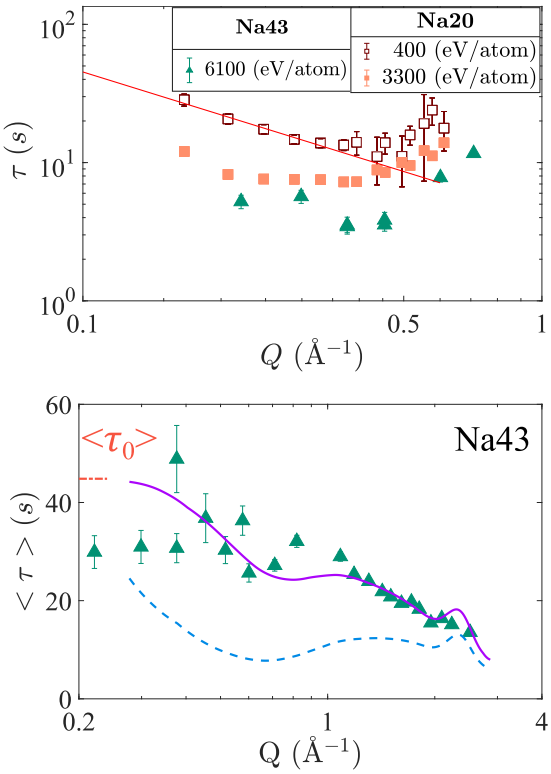


FIG. 6. (upper) Relaxation time as a function of the wave vector at low values and for Na20 (orange squares) and Na43 (green triangles). Data with empty symbols report the dynamics at low doses which is displayed only for Na20, while the full points report the results in the high-dose regime. (lower) Average relaxation time as a function of the wave vector for the Na43 sample at high doses. The blue dotted line is the prediction of the diffusive-like model reported in Eq. (6). The magenta line represents the model described in Eq. (7), which has been optimized on the shown data. The dash-dotted red line is placed at the value of the $\langle\tau_0\rangle$ parameter of Eq. (7).

decorrelation time with Q in the pristine glass. The β value on the peak of the $S(Q)$ is compatible with the stretched shape of the correlation curves reported in the previous study [27].

It is worth noticing that the low-Q beamline configuration used in this paper allowed us to reach Q values as small as 0.2 Å^{-1}, extending the range of the usual wide-angle XPCS measurements. The typical wide-angle setup is limited to wave vectors higher than 0.5 Å^{-1} because of the spurious signal at small angles coming from the Kapton windows of the sample environment, windows that here were removed. The low-Q region is plotted in a log-log scale in the upper panel of Fig. 6 for both samples. The dynamics of Na43 is reported only in the high-dose regime (full green triangles) because of the large uncertainty in the data at low dose, while that of Na20 is shown both in the low-dose (empty brown squares) and high-dose (full orange squares) ranges. In the low-dose regime, the relaxation time of Na20 decreases between 0.15 and 0.4 Å^{-1}, with a power law $\tau = Q^{-\alpha}$ with $\alpha = 1.0 \pm 0.1$. This behavior is typical of a ballisticlike motion, although here, the value of β is significantly lower than 1, while the usual ballistic motion is associated to a compressed exponential.

IV. DISCUSSION

The wave vector dependence of the relaxation time in the high-Q regime for both samples is reminiscent of a de Gennes narrowing process, where τ increases in correspondence of the FSDP of the glass and presents an oscillatory behavior at higher Q's. de Gennes investigated the relaxation time measured in quasielestic neutron scattering experiments of simple liquids, where τ is in the subpicosecond range [44]. The underlying idea to the model is that one can retrieve information on the intermediate scattering function $F(Q,t)$ from its self component $F_s(Q,t)$ at sufficiently high Q values since both will converge to the single-particle regime at high Q's. The proposed scaling model postulates that

$$F(Q,t) = S(Q)F_s(Q/\sqrt{S(Q)},t). \tag{5}$$

This relationship preserves the zeroth- and second-order sum rules for the dynamic structure factor. Within this approximation and assuming a diffusivelike process, one then expects τ to follow the law:

$$\tau_s = \frac{S(Q)}{DQ^2}, \tag{6}$$

where D is an effective diffusion constant. In our case, D is dose rate dependent since the observed dynamics is beam induced. We apply the subscript s to τ here to highlight the fact that it is derived from the self part of the intermediate scattering function. A diffusionlike model modified by the inclusion of $S(Q)$ as in Eq. (6) has been successfully exploited in a selection of borate glasses [31]. The comparison between $\tau(Q)$ and $S(Q)/Q^2$ is presented in Fig, 4 for Na43 and Fig. 5 for Na20 (for this sample, the same comparison is reported in Ref. [27]). In Na43, τ is peaked at $Q \sim 1$ Å^{-1} and $Q \sim 2.3$ Å^{-1}. Equation (6) can capture this oscillatory behavior in a qualitative way at high Q's.

However, the equation does not represent the observed dynamics in the low-Q range, i.e., for $Q \lesssim 0.6$ Å^{-1}. Here, $S(Q)$ is approximately constant, and the diffusion model would predict $\tau \propto Q^{-2}$ in contrast with our data. The discrepancy is very visible in the bottom panel of Fig, 6, where we report the average relaxation time $\langle\tau\rangle$ expressed as $\langle\tau\rangle{=}\Gamma(1/\beta)\tau/\beta$ [45]. The observed dynamics in this low-Q regime is dominated by collective density fluctuations, not considered in the simple diffusionlike model.

One of the main results of this paper is the observation of a Q-independent relaxation time at low Q for both the analyzed glasses in the high-dose regime, as shown in the upper panel of Fig. 6. The presence of a finite τ at small Q's together with the stretched shape of the correlation function ($\beta < 1$) is an indication that the irradiated glass behaves as a liquid in the high-dose regime, strengthening the previously reported observation [33]. A similar behavior with Q and dose has been reported recently by some of us in the case of a lithium metaborate glass and in the corresponding supercooled liquid [34]. These observations indicate that the induced dynamics at these doses is collective.

A tentative interpolation formula to bridge the high- and low-Q regimes can be introduced in the following way. It is well known from studies on simple liquids [46] that Eq. (5) cannot work at low Q's. A generalized hydrodynamics

approach suggests a transition from the low-Q range, where τ has a finite value comparable with the Maxwell relaxation time [47], to the high-Q regime, with an appropriate interpolation formula [46]. We recast it here in the following form:

$$\frac{1}{\tau(Q)^2} = \frac{1}{\tau_s(Q)^2} + \left(1 + \frac{Q^2}{Q_c^2}\right)^{-1}\left[\frac{1}{\tau_0^2} - \frac{1}{\tau_s(Q)^2}\right], \quad (7)$$

where $\tau_s(Q)$ is given by Eq. (6), τ_0 is the value of τ for $Q = 0$, and Q_c is a wave vector that separates the low-Q from the high-Q regimes. We fixed $Q_c = 2.5\,\text{Å}^{-1}$, the position of the sharp diffraction peak for Na43, following the literature on simple liquids [46]. The parameters D and τ_0 are optimized by a χ^2 minimization routine to the values of $\langle\tau(Q)\rangle$ of Na43, giving the values: $D = 0.018(1)\,\text{Å}^2/\text{s}$ and $\langle\tau_0\rangle = 44(5)$ s. The resulting curve is reported in the bottom panel of Fig. 6. The agreement with the data is pretty good and highlights the limitations of an approach based on a diffusionlike model and the need to consider the low-Q hydrodynamic regime, where τ should match its macroscopic value. We stress again that the probed τ is dose rate dependent so that the glass is liquidlike only when illuminated by the x-ray beam, while it is a solid when the beam is off.

We would like now to briefly discuss the evolution of the stretching parameter β as a function of dose in the two studied samples. The parameter β is slightly higher than 1 for some Q values around the FSDP in the pristine Na43 glass, as shown in Fig. 4. The compressed exponential shape is commonly observed in oxide glasses probed by XPCS. A lively debate is still ongoing in the literature concerning the interpretation of the nature of this peculiar shape of the correlation function. In soft systems, this shape is attributed to stress release mechanisms at the microscopic level [20]. In oxide glasses, as discussed in recent papers [26,34], the defects in the glass network are generated by the x-ray beam and give rise to elastic dipoles with a strain field that extend in space with a power-law tail. The observed density relaxations are governed by the response of the material in the presence of these dipoles and can show compressed correlation functions [48] as well as a different kind of atomic dynamics [26,34], with an evolution as a function of the dose that follows the parallel structural modification [34]. In the high-dose regime, both samples studied here show a stretched exponential behavior in the entire investigated wave vector range with β approximately following the shape of $S(Q)$, in agreement with the previously discussed de Gennes narrowing.

The β values of Na20 at low doses deviate from this trend, being <1 at all Q's. We can advance two different interpretations of this behavior. The stretched shape of the correlation curve could result from the dose accumulation, which is not negligible with respect to the dose required to change the structure of the glass. In the low-Q regime, the x-ray dose of the pristine glass ($\sim$60 s of irradiation) is comparable with the time τ_I, as shown in the inset of the upper panel of Fig. 5. An alternative explanation is based on the observation that this composition with 20% of Na_2O is considered the isostatic point of the sodium silicate glasses [49], and it should present a lower level of elastic stress in the pristine glass with respect to the other compositions. The role of the native defect population in the beam induced process is, however, unclear at the moment, and we consider the first interpretation to be more convincing.

V. CONCLUSIONS

We have probed the Q dependence of the XPCS correlation curves of two sodium silicate glasses. The x-ray dose accumulation induces an evolution from the pristine sample to a new amorphous state, through subsequent radiolytic events. The dynamics follows the structural evolution with a reduction of the observed relaxation time and of the stretching parameter. In the high-Q range, the observed dynamics shows indication of the presence of de Gennes narrowing at both the low and high radiation doses considered here.

Our setup has enabled the investigation of the low-Q regime, where we have found for the Na20 sample a ballistic dynamics with $\tau \propto Q^{-1}$ at short exposures and a gradual weakening of this Q dependence at long exposures. In both samples, the relaxation time is Q independent at long exposures, i.e., in the final amorphous state. The presence of a finite τ at low Q can be ascribed to the existence of independent relaxing units with dimensions smaller than the one probed in the experiment.

This paper is a pathway for future investigations in this low-Q region, in which XPCS can be exploited as a tool to probe the heterogeneous elastic response of amorphous materials. Revealing the heterogeneous nature of the elastic response of a glass at the nanometer scale is of great relevance both for fundamental and applied research, for example, in the realization of nonvolatile memories [50] or for neuromorphic devices [51], a field in which amorphous chalcogenides are promising candidates as phase change materials [52].

ACKNOWLEDGMENTS

The research in this paper was carried out at beamline P10 during Experiment No. I-20180946 at DESY, a member of the Helmholtz Association. The research activity was supported by the project CALIPSOplus under Grant Agreement No. 730872 from the EU Framework Program for Research and Innovation HORIZON 2020.

[1] G. Baldi, A. Fontana, and G. Monaco, Vibrational dynamics of non-crystalline solids, in *Low-Temperature Thermal and Vibrational Properties of Disordered Solids: A Half-Century of Universal Anomalies of Glasses* (World Scientific, Singapore, 2023), pp. 177–226.

[2] G. Baldi, G. Carini Jr, G. Carini, A. Chumakov, R. Dal Maschio, G. D'Angelo, A. Fontana, E. Gilioli, G. Monaco, L. Orsingher *et al.*, New insights on the specific heat of glasses, Philos. Mag. **96**, 754 (2016).

[3] G. Monaco and V. M. Giordano, Breakdown of the Debye approximation for the acoustic modes with nanometric wavelengths in glasses, Proc. Natl. Acad. Sci. USA **106**, 3659 (2009).

[4] G. Baldi, V. M. Giordano, G. Monaco, and B. Ruta, Sound attenuation at terahertz frequencies and the boson peak of vitreous silica, Phys. Rev. Lett. **104**, 195501 (2010).

[5] G. Baldi, M. Zanatta, E. Gilioli, V. Milman, K. Refson, B. Wehinger, B. Winkler, A. Fontana, and G. Monaco, Emergence of crystal-like atomic dynamics in glasses at the nanometer scale, Phys. Rev. Lett. **110**, 185503 (2013).

[6] G. Baldi, V. M. Giordano, B. Ruta, and G. Monaco, On the nontrivial wave-vector dependence of the elastic modulus of glasses, Phys. Rev. B **93**, 144204 (2016).

[7] L. Hong, V. N. Novikov, and A. P. Sokolov, Dynamic heterogeneities, boson peak, and activation volume in glass-forming liquids, Phys. Rev. E **83**, 061508 (2011).

[8] H. Mizuno, S. Mossa, and J.-L. Barrat, Measuring spatial distribution of the local elastic modulus in glasses, Phys. Rev. E **87**, 042306 (2013).

[9] H. Wagner, D. Bedorf, S. Kuechemann, M. Schwabe, B. Zhang, W. Arnold, and K. Samwer, Local elastic properties of a metallic glass, Nat. Mater. **10**, 439 (2011).

[10] G. Baldi, V. M. Giordano, B. Ruta, R. Dal Maschio, A. Fontana, and G. Monaco, Anharmonic damping of terahertz acoustic waves in a network glass and its effect on the density of vibrational states, Phys. Rev. Lett. **112**, 125502 (2014).

[11] A. Widmer-Cooper, H. Perry, P. Harrowell, and D. R. Reichman, Irreversible reorganization in a supercooled liquid originates from localized soft modes, Nat. Phys. **4**, 711 (2008).

[12] L. Berthier, G. Biroli, J.-P. Bouchaud, L. Cipelletti, and W. van Saarloos, *Dynamical Heterogeneities in Glasses, Colloids, and Granular Media* (Oxford University Press, Oxford, 2011), Vol. 150.

[13] L. E. Bove, E. Fabiani, A. Fontana, F. Paoletti, C. Petrillo, O. Pilla, and I. C. V. Bento, Brillouin neutron scattering of v-GeO_2, Europhys. Lett. **71**, 563 (2005).

[14] G. Baldi, A. Fontana, G. Monaco, L. Orsingher, S. Rols, F. Rossi, and B. Ruta, Connection between boson peak and elastic properties in silicate glasses, Phys. Rev. Lett. **102**, 195502 (2009).

[15] M. Zanatta, G. Baldi, S. Caponi, A. Fontana, C. Petrillo, F. Rossi, and F. Sacchetti, Debye to non-Debye scaling of the boson peak dynamics: Critical behavior and local disorder in vitreous germania, J. Chem. Phys. **135**, 174506 (2011).

[16] D. Sidebottom, R. Bergman, L. Börjesson, and L. M. Torell, Two-step relaxation decay in a strong glass former, Phys. Rev. Lett. **71**, 2260 (1993).

[17] J. H. Wu and Q. Jia, The heterogeneous energy landscape expression of KWW relaxation, Sci. Rep. **6**, 20506 (2016).

[18] M. D. Ediger, C. A. Angell, and S. R. Nagel, Supercooled liquids and glasses, J. Phys. Chem. **100**, 13200 (1996).

[19] L. Ramos and L. Cipelletti, Ultraslow dynamics and stress relaxation in the aging of a soft glassy system, Phys. Rev. Lett. **87**, 245503 (2001).

[20] L. Cipelletti, S. Manley, R. C. Ball, and D. A. Weitz, Universal aging features in the restructuring of fractal colloidal gels, Phys. Rev. Lett. **84**, 2275 (2000).

[21] D. Orsi, L. Cristofolini, G. Baldi, and A. Madsen, Heterogeneous and anisotropic dynamics of a 2D gel, Phys. Rev. Lett. **108**, 105701 (2012).

[22] D. Orsi, B. Ruta, Y. Chushkin, A. Pucci, G. Ruggeri, T. Baldi, G. Rimoldi, and L. Cristofolini, Controlling the dynamics of a bidimensional gel above and below its percolation transition, Phys. Rev. E **89**, 042308 (2014).

[23] M. Bouzid, J. Colombo, L. V. Barbosa, and E. Del Gado, Elastically driven intermittent microscopic dynamics in soft solids, Nat. Commun. **8**, 15846 (2017).

[24] J.-P. Bouchaud and E. Pitard, Anomalous dynamical light scattering in soft glassy gels, Eur. Phys. J. E **6**, 231 (2001).

[25] B. Ruta, F. Zontone, Y. Chushkin, G. Baldi, G. Pintori, G. Monaco, B. Ruffle, and W. Kob, Hard x-rays as pump and probe of atomic motion in oxide glasses, Sci. Rep. **7**, 3962 (2017).

[26] F. Dallari, A. Martinelli, F. Caporaletti, M. Sprung, G. Baldi, and G. Monaco, Stochastic atomic acceleration during the x-ray-induced fluidization of a silica glass, Proc. Natl. Acad. Sci. USA **120**, e2213182120 (2023).

[27] B. Ruta, G. Baldi, Y. Chushkin, B. Rufflé, L. Cristofolini, A. Fontana, M. Zanatta, and F. Nazzani, Revealing the fast atomic motion of network glasses, Nat. Commun. **5**, 3939 (2014).

[28] G. Pintori, G. Baldi, B. Ruta, and G. Monaco, Relaxation dynamics induced in glasses by absorption of hard x-ray photons, Phys. Rev. B **99**, 224206 (2019).

[29] F. Dallari, G. Pintori, G. Baldi, A. Martinelli, B. Ruta, M. Sprung, and G. Monaco, X-rays induced atomic dynamics in a lithium-borate glass, Condens. Matter Phys. **22**, 43606 (2019).

[30] A. Martinelli, G. Baldi, F. Dallari, B. Rufflé, F. Zontone, and G. Monaco, Probing the dynamics of B_2O_3 across the glass transition: An x-ray photon correlation spectroscopy study, Philos. Mag. **100**, 2636 (2020).

[31] K. Holzweber, C. Tietz, T. M. Fritz, B. Sepiol, and M. Leitner, Beam-induced atomic motion in alkali borate glasses, Phys. Rev. B **100**, 214305 (2019).

[32] G. Pintori, G. Baldi, F. Dallari, A. Martinelli, M. Sprung, and G. Monaco, X-ray induced dynamics in borate glasses with different network connectivity, Phys. Rev. B **105**, 104207 (2022).

[33] E. Alfinelli, F. Caporaletti, F. Dallari, A. Martinelli, G. Monaco, B. Ruta, M. Sprung, M. Zanatta, and G. Baldi, Amorphous-amorphous transformation induced in glasses by intense x-ray beams, Phys. Rev. B **107**, 054202 (2023).

[34] A. Martinelli, F. Caporaletti, F. Dallari, M. Sprung, F. Westermeier, G. Baldi, and G. Monaco, Reaching the yield point of a glass during x-ray irradiation, Phys. Rev. X **13**, 041031 (2023).

[35] N. P. Bansal and R. H. Doremus, *Handbook of Glass Properties* (Academic Press, Inc., Orlando, 1986).

[36] B. L. Henke, E. M. Gullikson, and J. C. Davis, X-ray interactions: Photoabsorption, scattering, transmission, and reflection at $E = 50$–$30,000$ eV, $Z = 1$–92, At. Data Nucl. Data Tables **54**, 181 (1993).

[37] H. Jabraoui, Y. Vaills, A. Hasnaoui, M. Badawi, and S. Ouaskit, Effect of sodium oxide modifier on structural and elastic properties of silicate glass, J. Phys. Chem. B **120**, 13193 (2016).

[38] A. Madsen, A. Fluerasu, and B. Ruta, Structural dynamics of materials probed by x-ray photon correlation spectroscopy, in *Synchrotron Light Sources and Free-Electron Lasers*, edited by

E. Jaeschke, S. Khan, J. Schneider, and J. Hastings (Springer, Cham, 2020), pp. 1989–2018.

[39] B. Ruta, G. Monaco, V. M. Giordano, F. Scarponi, D. Fioretto, G. Ruocco, K. S. Andrikopoulos, and S. N. Yannopoulos, Nonergodicity factor, fragility, and elastic properties of polymeric glassy sulfur, J. Phys. Chem. B **115**, 14052 (2011).

[40] T. Scopigno, G. Ruocco, F. Sette, and G. Monaco, Is the fragility of a liquid embedded in the properties of its glass? Science **302**, 849 (2003).

[41] D. L. Sidebottom, B. V. Rodenburg, and J. R. Changstrom, Connecting structure and dynamics in glass forming materials by photon correlation spectroscopy, Phys. Rev. B **75**, 132201 (2007).

[42] B. Hehlen, D. R. Neuville, D. Kilymis, and S. Ispas, Bimodal distribution of Si–O–Si angles in sodo-silicate glasses, J. Non-Cryst. Solids **469**, 39 (2017).

[43] C. Levelut, R. Le Parc, A. Faivre, R. Brüning, B. Champagnon, V. Martinez, J.-P. Simon, F. Bley, and J.-L. Hazemann, Density fluctuations in oxide glasses investigated by small-angle x-ray scattering, J. Appl. Cryst. **40**, s512 (2007).

[44] P. G. De Gennes, Liquid dynamics and inelastic scattering of neutrons, Physica **25**, 825 (1959).

[45] A. Arbe and J. Colmenero, Characterization of the simple-liquid state in a polymeric system: Coherent and incoherent scattering functions, Phys. Rev. E **80**, 041805 (2009).

[46] J. P. Boon and S. Yip, *Molecular Hydrodynamics* (Dover Publications, Inc., New York, 1991).

[47] R. D. Mountain, Relaxation times for the volume viscosity of simple fluids, J. Chem. Phys. **48**, 2189 (1968).

[48] G. Rodriguez-Lopez, K. Martens, and E. E. Ferrero, Temperature dependence of fast relaxation processes in amorphous materials, Phys. Rev. Mater. **7**, 105603 (2023).

[49] M. Bauchy, Deciphering the atomic genome of glasses by topological constraint theory and molecular dynamics: A review, Comput. Mater. Sci. **159**, 95 (2019).

[50] C. S. Hwang, Prospective of semiconductor memory devices: From memory system to materials, Adv. Electron. Mater. **1**, 1400056 (2015).

[51] G. Baldi, S. Battistoni, G. Attolini, M. Bosi, C. Collini, S. Iannotta, L. Lorenzelli, R. Mosca, J. S. Ponraj, R. Verucchi *et al.*, Logic with memory: And gates made of organic and inorganic memristive devices, Semicond. Sci. Technol. **29**, 104009 (2014).

[52] M. Wuttig, H. Bhaskaran, and T. Taubner, Phase-change materials for non-volatile photonic applications, Nat. Photon. **11**, 465 (2017).